



Role of Inter-site Hubbard Interactions in MnS Monolayer: DFT+U+V Investigation

Yusuf Zuntu ABDULLAHI^{1,2*}

¹ Department of Physics, Adnan Menderes University, Aydın 09010, Türkiye

² Department of Physics, Faculty of Science, Kaduna State University, P.M.B. 2339 Kaduna State, Nigeria

Highlights

- Tetragonal MnS monolayer has been investigated using DFT+U +V calculations.
- The MnS monolayer prefers an in-plane easy axis for the MAE.
- The estimated BKT transition temperature is as high as 1667.8 K.
- The estimated carrier mobility of holes and electrons are $2.12 \text{ cm}^2 \text{ v}^{-1} \text{ S}^{-1}$ and $1.21 \text{ cm}^2 \text{ v}^{-1} \text{ S}^{-1}$.

Article Info

Received: 31 May 2023

Accepted: 07 Dec 2023

Keywords

MnS monolayer,
Formation energy,
Electronic and magnetic
properties,
BKT transition
temperature

Abstract

The stable MnS monolayer was recently predicted using first-principles density functional theory (DFT) including Hubbard U (DFT+U) correction and Monte Carlo (MC) simulations. It is shown to exhibit an indirect band gap of 0.68 eV semiconductor with a high Neel temperature (T_N) of 720 K and an in-plane easy axis magnetic anisotropy energy (MAE). The considered on-site Hubbard U correction takes into account only the Mn (3d) localized nature. To correct the inter-site errors due to strong hybridization between bonded Mn (3d) and S (2p) states, the Hubbard +V inter-site parameter should be added to the calculations. In this study, the band gap of MnS is found to be increased to 1.24 eV (twice that for DFT+U) after considering the inter-site V correction (DFT+U+V). Since the MnS monolayer prefers an in-plane easy axis for the MAE, the estimated Berezinskii-Kosterlitz-Thouless transition (BKT) transition temperature is as high as 1667.8 K. The carrier mobility is calculated based on the deformation potential and effective mass and it is found that holes ($2.12 \text{ cm}^2 \text{ v}^{-1} \text{ S}^{-1}$) are twice the size of these electrons ($1.21 \text{ cm}^2 \text{ v}^{-1} \text{ S}^{-1}$). The results are expected to improve the potential of the MnS monolayers in multiple AFM spintronic device applications.

1. INTRODUCTION

Following the experimental synthesis of transition metal (TM) boride (MBene) in Cr_2B_2 monolayer form [1], considerable attention is focused on various MBene-like structures. These newly designed structures have been reported to hold promise for batteries, superconducting and spintronics applications [2–7]. For example, the titanium boron nitride (Ti_2BN) monolayer is found to be suitable for Li-ion batteries (LIBs) with a capacity of about 889 mAhg^{-1} and a 165 meV diffusion barrier of Li-ion on the Ti_2BN surface [3]. The ferromagnetic MnX ($X = \text{As}, \text{P}$) monolayers [2] with semimetallic properties have been reported to be suitable for high Curie temperature (T_C) spintronic devices using DFT [8] plus on-site U Hubbard correction (DFT+U) [9]. Moreover, the Mn_2B_2 monolayer shows metallic ferromagnetism properties with T_C of 406 K, well above room temperature [7]. Following this trend, we found an indirect narrowed bandgap of 0.23 eV and a high T_N of the VP monolayer up to 1263 K with an in-plane magnetic anisotropy energy (MAE) using DFT+U calculations and the mean-field approximation [10]. In another separate study, MnS monolayer was found to have antiferromagnetic (AFM) semiconducting properties and a high T_N of 720 K. It was also shown to exhibit an in-plane magnetic anisotropy of $E([001]) - E[110] = 0.39 \text{ meV}$ [11].

Among these studied MBene-like structures, the *MnS* monolayer is particularly unique. Instead of metallic property (DFT), DFT+U results show semiconducting properties (band gap of about 0.68 eV), similar to the metal-to-semiconductor transition associated with *VP* sheet [10]. The metal to semiconductor transition in *MnS* shows that self-interaction error of partially filled 3d of Mn atom has been corrected by adding the on-site Hubbard U parameter. The reported Hubbard U of 3.33 eV was obtained based on DFT linear response approach (LRA) [9]. However, since there is no experimental report on the *MnS* monolayer and the fact that it contains a wealth of new information that still needs to be explored, there is a need for more detailed studies of ground state properties. Additionally, since the *MnS* monolayer has an in-plane MAE, it should correspond to the XY-model, which is expected to feature novel transitions, such as the BKT transition temperature suitable for superfluid spin transport. Therefore, this study aimed to revisit the ground state properties of the *MnS* monolayer using the recently developed and most reliable DFT+U+V method [12, 13]. The method includes the inter-site Hubbard parameter, which accounts for the strong hybridization between neighboring Mn (3d) and S (p) atoms. The DFT+U+V method has been successfully used to access the correct ground state properties of TM involved structures that is consistent with the experimental results [14, 15]. In the current study, the calculated band gap for *MnS* monolayers increases with the DFT+U+V (1.24 eV) method compared to DFT+U (0.68 eV) calculations. The BKT temperature value of the *MnS* monolayer is as high as 1667.8 K. The calculated room temperature holes mobility in the *MnS* monolayer is about twice that of electrons.

2. COMPUTATIONAL METHOD

This study used spin-polarized DFT+U+V [8, 12, 13] method as carried out with the aid of Quantum Espresso (QE) simulation package [16] to investigate the ground state properties of the *MnS* monolayer. The exchange and correlation energies of the strongly localized 3d orbital of the Mn atom has been treated using the generalized gradient approximation of Perdew-Burkew-Enzerhof (PBE) combined including the Hubbard U+V parameters. The U+V value for the *MnS* monolayer has been evaluated self-consistently from the ab-initio method using the LRA method [9], which has been conceptualized based on density-functional perturbation theory (DFPT) [13]. The estimated U+V value for *MnS* monolayer is 4.47 eV. The calculations have been performed using Lowdin-orthogonalized atomic orbitals [17] and the Hubbard projector so that they correspond well with the projected augmented wave (PAW) [18]. The method for estimating the U+V Hubbard parameters followed the same as that in earlier investigations [14, 15], and DFPT calculations were implemented using the HP code [19] in the QE package [19]. The electron-ion core has been treated using the PAW pseudopotentials method [18]. The van der Waals (vdW) dispersion correction of the Grimme D2 [20] approach of PBE functionals (PBE+D2) has been used in all calculations. The kinetic energy cutoff of 500 eV was employed for the plain wave basis set. To aid in integral convergences, Marzari-Vanderbilt smearing with Gaussian spreading has been considered [21]. The $12 \times 12 \times 1$ and $16 \times 16 \times 1$ Monkhorst-Pack k-point meshes [22] have been used for Brillouin zone (BZ) integration for total energy and total density of states (TDOS) calculations, respectively. The simulation cell has included a thick vacuum layer of 16 Å perpendicular to the *MnS* monolayer to avoid interactions of periodic images.

3. RESULTS AND DISCUSSION

This theoretical investigation extends the predicted semiconducting *MnS* monolayer with an AFM ground state (PBE+U and MC calculations) by examining the effects of inter-site Hubbard V correction on the electronic and magnetic properties. To produce similar lattice parameters, we ensure that computational method such as PAW-PP and PBE have been used for the QE package calculations, as previously reported using the VASP [11]. Hence, the reproduced optimized structure of the *MnS* monolayer with an AFM ground state is determined and displayed in Figure 1 (a). The lattice constant ($a=b= 3.378$ Å (PBE) and $a=b= 3.73$ Å (PBE+U)) value decreased to $a=b= 3.605$ Å when the inter-site V Hubbard correction is added (PBE+U+V). This shows that the inter-site correction creates strong atomic bonding in the *MnS* monolayer as reflected by the lowered lattice constant value. The decreased lattice constant value is expected to affect the electronic and magnetic properties of the *MnS* monolayer.

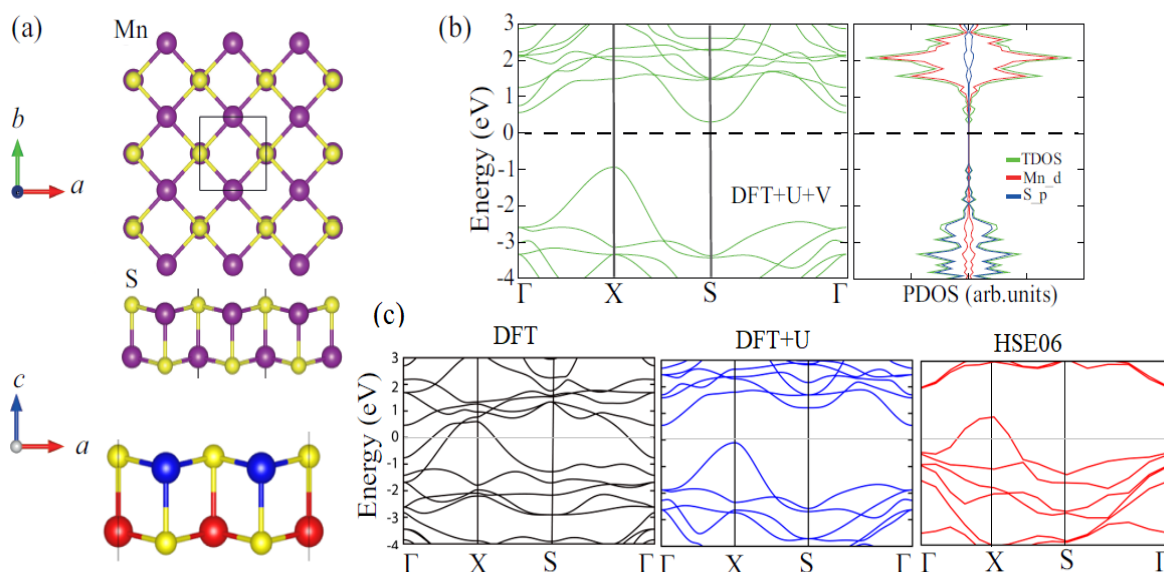


Figure 1. (a) Typical structure of MnS monolayer. Blue and red colors of MnS side view represent the spin up and spin down, respectively. (b) Left: The electronic band structure of the MnS monolayer obtained using PBE+U+V method. Right: represent the total and partial density of states of the MnS monolayer. (c) From left to right, the plots show electronic band structure of the MnS monolayer obtained using PBE, PBE+U and HSE06 methods

previously reported [11], the preferred AFM configuration is the one with parallel spins within each portion of the Mn atom but opposite spins in the upper and lower portions of the Mn atoms (See side view of MnS monolayer in Figure 1 (a)). For this AFM configuration, the total magnetic moment is zero, which means no redundant magnetic field will interact with the external magnetic field. It should be emphasized that the superexchange interaction between Mn ions linked through the S ion is the main cause of the MnS AFM ground state. Based on the Goodenough-Kanamori-Anderson rule, AFM coupling is favored for $90^\circ > \theta > 90^\circ$ superexchange interactions between two Mn ions. Thus, this large overlap integral L favored a non-orthogonal spatial interaction between the Mn-d orbital and the p orbital of S ions. Consequently, the exchange integral J should be expressed as $J = 4\beta L$ (β represent the hopping integral), leading to the AFM ground state of the MnS monolayers.

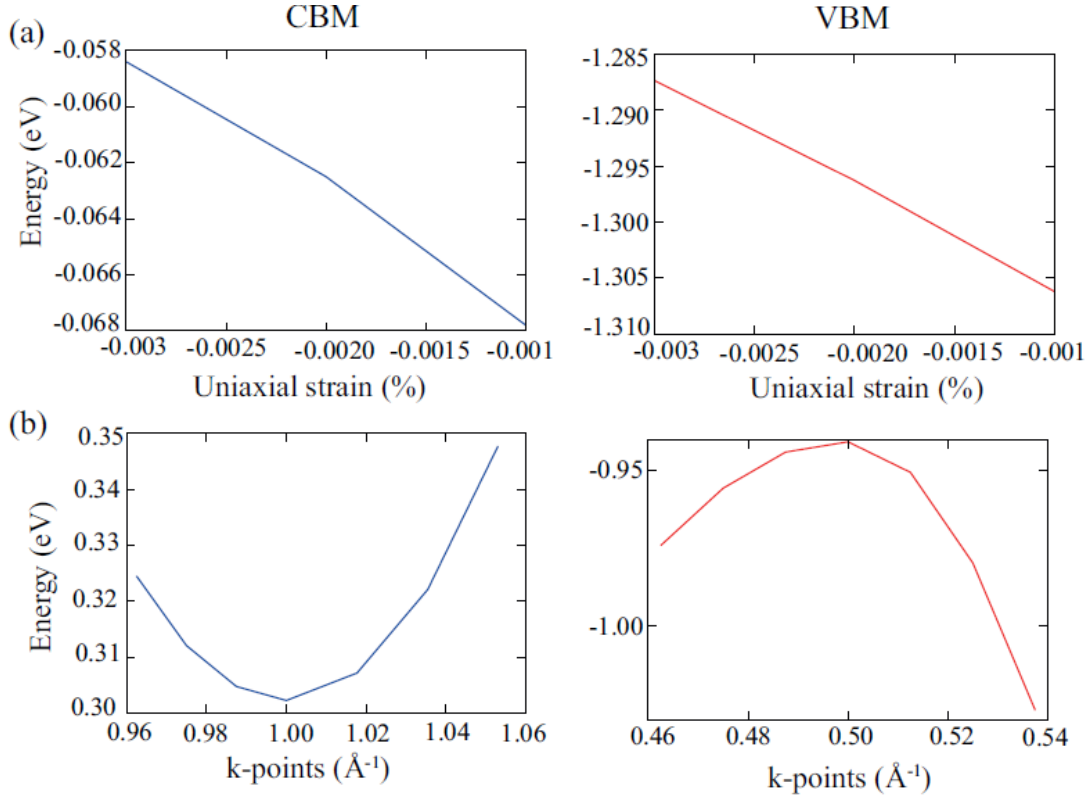


Figure 2. a) The shift of CBM and VBM versus uniaxial strain along the strain directions and b) the E vs k points near the CBM and VBM plots

Having determined the MnS -AFM ground-state structure, it is crucial to investigate the energetic feasibility of this MnS monolayer by calculating its formation energy (E_{FE}), since the dynamic, mechanical, and thermal stabilities have been previously ascertain [11]. The thermodynamic (E_{FE}) per atom is estimated with the PBE method using the expression given by

$$E_{FE} = (E_{Mn_2S_2} - 2\mu_{Mn} - 2\mu_S)/4. \quad (1)$$

Here μ_{Mn} , and μ_S stand for the chemical potentials of Mn and S atoms, respectively. The μ_{Mn} , and μ_S are determined from the expression given as $\mu_{Mn \text{ or } S} = (E_{Mn \text{ or } S})/n$, where n is the number of Mn and S atoms in their bulk phases. The bulk Mn and S structures with space group I41/amd and P2/c respectively are available online in material projects. The estimated E_{FE} value is -0.612 eV/atom for MnS monolayer. The negative E_{FE} value is illustrating that the MnS monolayer is thermodynamically stable and might be experimentally synthesized.

It is worth noting that the previous report [11] shows that the MnS monolayer exhibits metallic properties at the PBE (HSE06) level and an indirect band gap of 0.68 eV at the PBE+U level (See Figure 1 (c)). Interestingly, the indirect bandgap increases to 1.24 eV when the inter-site Hubbard V correction is included. Also, the positions of CBM and VBM alternate as a result of Inter-site V correction. This corresponds to the shift of VBM and CBM to higher energy, and the band gap increases, as shown in Figure 1 (b). The partial density of states (PDOS) plot shows dominant features of Mn d and S p orbital contributions in CBM and VBM, respectively. As clearly shown in Figure 2, both CBM and VBM have relatively broad curvature energy bands, indicating increased effective masses of both holes and electrons. This significant localization of electrons and holes can lead to large correlation effects [23] corresponding to unusual phenomena such as room temperature FM/AFM [24, 25] and the fractional quantum Hall effect [26]. According to the previously reported PDOS [11], the Mn (3d) and p of the S orbitals have dominant contributions in CBM and VBM respectively, which are comparable to the PDOS plot in Figure 1 (b) obtained in the current study using PBE+U+ V method. Thus, the physical reason for the increased band

gap (1.24 eV) for the PBE+U+V method compared to the 0.68 eV of the PBE+U method is related to the shift of CBM towards the Fermi level while the VBM moves away from the Fermi level (See Figure 1 (c)). This means that the intersite Hubbard V correction promotes localized impurities near the Fermi energy as a result of the reduced lattice constant value, which widens the band gap. Using PBE+U+V, the carrier mobility (μ) of the *MnS* monolayer is then estimated according to the expression given by;

$$\mu = \frac{2eh^3C}{3k_B T |m^*|^2 E_d^2} \quad (2)$$

where C and k_B denote the in-plane stiffness and Boltzmann constant. T and \hbar represent the room temperature (300 K) and reduced plank constant. The k_B is given as $1.38064852 \times 10^{-23} \text{ J K}^{-1}$. The deformation potential (E_d) [27] is evaluated from the slope of CBM and VBM energies versus small uniaxial strains along the direction. The strain-energy versus strain ration has been determined by $E = \frac{a_i - a_0}{a_0}$, a_i and a_0 represent strained and strained-free lattice constants (See Figure 2 (a)). The effective mass $m^* = \pm \hbar^2 \left(\frac{d^2 E_k}{dk^2} \right)^{-1}$ is evaluated from the fitted data set of $E - k$ curves (See Figure 2). The m^* values for electrons and holes are 9.36 and 3.54, indicating that the electrons are heavier than holes for the *MnS* monolayer. Therefore the calculated μ for electrons and holes in this *MnS* monolayer are $1.212 \text{ cm}^2 \text{ v}^{-1} \text{ s}^{-1}$ and $2.119 \text{ cm}^2 \text{ v}^{-1} \text{ s}^{-1}$ respectively. The mobility of the holes are twice the size of these electrons mainly due to the wider curvature band energy at the CBM.

Previous studies reported that *MnS* monolayer exhibits an in-plane MAE, serving as a typical case of the Heisenberg model limit. This is attributed to the fact that the Mermin-Wagner theorem mentions that isotropic magnetic monolayer with continuous spin symmetry in the plane, e.g. B. *MnS*, can not have long-range order at a finite temperature [28]. This implies that the magnetic state of the *MnS* monolayer belongs to the XY model and exhibits a very unique low-temperature BKT transition [29]. This phenomenon has been observed in *WXBC* ($X = Mn, Fe$) sheets [30]. Hence, the BKT can be estimated based on the XY model [31] defined as

$$T_N = 0.89(E_{FM} - E_{AFM})/8k_B \quad (3)$$

where $E_{AFM} - E_{FM}$ is calculated to be 1.292 eV per magnetic atoms. The calculated BKT temperature is 1667.8 K for the *MnS* monolayer. The BKT temperature value is well above the T_N (720 K) reported using MC simulations [11]. These novel magnetic properties of the *MnS* monolayer expand its opportunities in topological magnetic textures and superfluid spin transport applications [32, 33]. However, a recent published report [34] shows that finite-size 2D van der Waals magnets (2D flakes) break the Mermin-Wagner theorem that exchange interactions dominate 2D magnetism without the need for magnetic anisotropy.

4. SUMMARY

In conclusion, the ground state (GS) properties of *MnS* monolayer are investigated using DFT+U+V method. The *MnS* monolayer maintains an AFM GS with an enhanced bandgap of 1.24 eV, which is twice that obtained for PBE+U after considering the inter-site V correction (PBE+U+V). Using the deformation potential and effective mass, the carrier mobility of holes ($2.12 \text{ cm}^2 \text{ v}^{-1} \text{ s}^{-1}$) are twice the size of these electrons ($1.21 \text{ cm}^2 \text{ v}^{-1} \text{ s}^{-1}$). The estimated BKT transition temperature value of the *MnS* monolayer is as high as 1667.8 K. The PBE+U+V results provide extensive details of the *MnS* monolayer as a potential material for high-end spintronics devices.

ACKNOWLEDGEMENT

I would like to acknowledge TUBITAK ULAKBIM, High Performance and Grid Computing Center (Tr-Grid e-Infrastructure). I would like to thank Prof. Dr. Ethem Akturk and Prof. Dr. Olcay Uzengi Akturk and Associate Prof. Dr. Fatih Ersan.

CONFLICTS OF INTEREST

No conflict of interest was declared by the author.

REFERENCES

- [1] Zhang, H., Xiang, H., Dai, F.-z., Zhang, Z., Zhou, Y., “First demonstration of possible two-dimensional mbene crb derived from mab phase cr₂alb₂”, *Journal of Materials Science & Technology*, 34(11): 2022–2026, (2018).
- [2] Wang, B., Zhang, Y., Ma, L., Wu, Q., Guo, Y., Zhang, X., Wang, J., “Mnx (x= p, as) monolayers: a new type of two-dimensional intrinsic room temperature ferromagnetic half-metallic material with large magnetic anisotropy”, *Nanoscale*, 11(10): 4204–4209, (2019).
- [3] Wu, Y.-Y., Bo, T., Zhu, X., Wang, Z., Wu, J., Li, Y., Wang, B.-T., “Two-dimensional tetragonal ti₂bn: A novel potential anode material for li-ion batteries”, *Applied Surface Science*, 513: 145821, (2020).
- [4] Escamilla, R., Carvajal, E., Cruz-Irisson, M., Morales, F., Huerta, L., Verdin, E., “Xps study of the electronic density of states in the superconducting mo₂b and mo₂bc compounds”, *Journal of Materials Science*, 51(13): 6411–6418, (2016).
- [5] Bolvardi, H., Emmerlich, J., Music, D., von Appen J., Dronskowski, R., Schneider, J., “Systematic study on the electronic structure and mechanical properties of x₂bc (x= mo, ti, v, zr, nb, hf, ta and w)”, *Journal of Physics: Condensed Matter*, 25(4): 045501, (2012).
- [6] Barua P., Hossain, M., Ali, M., Uddin, M., Naqib, S., Islam, A., “Effects of transition metals on physical properties of m₂bc (m= v, nb, mo and ta): a dft calculation”, *Journal of Alloys and Compounds* 770: 523–534, (2019).
- [7] Abdullahi, Y. Z., Vatansever, Z. D., Akturk, E., Akıncı, U., Akturk, O. U., “A tetragonal phase mn₂b₂ sheet: a stable room temperature ferromagnet with sizable magnetic anisotropy”, *Physical Chemistry Chemical Physics*, 22(19): 10893–10899, (2020).
- [8] Hohenberg P., Kohn, W., “Inhomogeneous electron gas”, *Physical Review*, 136(3B): B864, (1964).
- [9] Cococcioni, M., De Gironcoli, S., “Linear response approach to the calculation of the effective interaction parameters in the lda+ u method”, *Physical Review B*, 71(3): 035105, (2005).
- [10] Abdullahi, Y. Z., Ahmad, S., Ibrahim, A. A., “Effects of the hubbard u correction on the electronic and magnetic properties of the tetragonal v₂p₂ sheet”, *RSC Advances*, 11(56): 35061–35068, (2021).
- [11] Abdullahi, Y. Z., Ersan, F., Vatansever, Z. D., Akturk, U., Akturk, O. U., “Exploring the potential of mnx (s, sb) monolayers for antiferromagnetic spintronics: A theoretical investigation”, *Journal of Applied Physics*, 128(11): 113903, (2020).

- [12] Timrov, I., Marzari, N., Cococcioni, M., “Hubbard parameters from density-functional perturbation theory”, *Physical Review B*, 98(8): 085127, (2018).
- [13] Timrov, I., Marzari, N., Cococcioni, M., “Self-consistent hubbard parameters from density-functional perturbation theory in the ultrasoft and projector-augmented wave formulations”, *Physical Review B*, 103(4): 045141, (2021).
- [14] Mahajan, R., Timrov, I., Marzari, N., Kashyap, A., “Importance of intersite hubbard interactions in β -mno₂: A first-principles dft+u+v study”, *Physical Review Materials*, 5(10): 104402, (2021).
- [15] Mahajan, R., Kashyap, A., Timrov, I., “Electronic structure and magnetism of pristine and fe-doped-mno₂ from density-functional theory with extended hubbard functionals”, arXiv preprint arXiv:2205.05977, (2022).
- [16] Giannozzi, P., Baroni, S., Bonini, N., Calandra, M., Car, R., Cavazzoni, C., Ceresoli, D., Chiarotti, G. L., Cococcioni, M., Dabo, M., et al., “Quantum espresso: a modular and open-source software project for quantum simulations of materials”, *Journal of Physics: Condensed Matter*, 21(39): 395502, (2009).
- [17] Mayer, I., “On howdin’s method of symmetric orthogonalization”, *International Journal of Quantum Chemistry*, 90(1): 63–65, (2002).
- [18] Kresse, G., Joubert, D., “From ultrasoft pseudopotentials to the projector augmented-wave method”, *Physical Review B*, 59(3): 1758, (1999).
- [19] Timrov, I., Marzari, N., Cococcioni, M., “Hp-a code for the calculation of hubbard parameters using densityfunctional perturbation theory”, arXiv preprint arXiv:2203.15684, (2022).
- [20] Grimme, S., Antony, J., Ehrlich, S., Krieg, H., “A consistent and accurate ab initio parametrization of density functional dispersion correction (dft-d) for the 94 elements h-pu”, *The Journal of Chemical Physics*, 132(15): 154104, (2010).
- [21] Marzari, N., Vanderbilt, D., De Vita, A., Payne, M., “Thermal contraction and disordering of the al (110) surface”, *Physical Review Letters*, 82(16): 3296, (1999).
- [22] Monkhorst, H. J., Pack, J. D., “Special points for brillouin-zone integrations”, *Physical Review B*, 13(12): 5188, (1976).
- [23] Bilitewski, T., Moessner, R., “Disordered flat bands on the kagome lattice”, *Physical Review B*, 98(23): 235109, (2018).
- [24] Abdullahi, Y. Z., Vatansever, Z. D., Ersan, F., Akinci, U., Akturk, O. U., Akturk, E., “Ferromagnetic tm₂bc (tm= cr, mn) monolayers for spintronic devices with high curie temperature”, *Physical Chemistry Chemical Physics*, 23(10): 6107–6115, (2021).
- [25] Abdullahi, Y. Z., Vatansever, Z. D., Akturk, E., Akinci, U., Akturk, O. U., “Novel two-dimensional crx₂ (x= cr, ru) metal for high neel temperature antiferromagnetic spintronics”, *Journal of Solid State Chemistry*, 302: 122427, (2021).
- [26] Bergman, D. L., Wu, C., Balents, L., “Band touching from real-space topology in frustrated hopping models”, *Physical Review B*, 78(12): 125104, (2008).
- [27] Bardeen, J., Shockley, W., “Deformation potentials and mobilities in non-polar crystals”, *Physical Review*, 80(1): 72, (1950).

- [28] Mermin, N. D., Wagner, H., “Absence of ferromagnetism or antiferromagnetism in one-or two-dimensional isotropic heisenberg models”, *Physical Review Letters*, 17(22): 1133, (1966).
- [29] Kosterlitz, J. M., Thouless, D. J., Ordering, metastability and phase transitions in two-dimensional systems”, *Journal of Physics C: Solid State Physics*, 6(7): 1181, (1973).
- [30] Abdullahi, Y. Z., Ahmad, S., Ersan, F., “Exploring room-temperature ferromagnetism in wxbc (x= w, mn, fe) monolayers”, *RSC Advances*, 12(44): 28433–28440, (2022).
- [31] Fern´andez, J. F., Ferreira, M. Stankiewicz, F., J., “Critical behavior of the two-dimensional xy model: A monte carlo simulation”, *Physical Review B*, 34(1): 292, (1986).
- [32] Augustin, M., Jenkins, S., Evans, R. F., Novoselov, K. S., Santos, E. J., “Properties and dynamics of meron topological spin textures in the two-dimensional magnet CrCl_3 ”, *Nature Communications*, 12(1): 1–9, (2021).
- [33] Takei, S., Tserkovnyak, Y., “Superfluid spin transport through easy-plane ferromagnetic insulators”, *Physical Review Letters*, 112(22): 227201, (2014).
- [34] Sarah, J., Rózsa, L., Atxitia, U., FL Evans, R., Novoselov, K. S., and JG Santos, E., “Breaking through the Mermin-Wagner limit in 2D van der Waals magnets”, *Nature Communications*, 13(1): 6917, (2022).

EARLY VIEW